Formation of quasi-periodic nano- and microstructures on silicon surface under IR and UV femtosecond laser pulses

A.A. Ionin, S.I. Kudryashov, S.V. Makarov, L.V. Seleznev, D.V. Sinitsyn,
E.V. Golosov, O.A. Golosova, Yu.R. Kolobov, A.E. Ligachev

Abstract. **Quasi-periodic nano- and microstructures have been formed on silicon surface using IR ($\lambda \approx 744$ nm) and UV ($\lambda \approx 248$ nm) femtosecond laser pulses. The influence of the incident laser fluence and the number of pulses on the structured surface topology has been investigated. The silicon nanostructuring thresholds have been determined for the above-mentioned wavelengths. Modulation of the surface relief at the doubled spatial frequency is revealed and explained qualitatively. The periods of the nanostructures formed on the silicon surface under IR and UV femtosecond laser pulses are comparatively analysed and discussed.**

Keywords: *IR and UV femtosecond laser pulses, silicon, surface quasi-periodic nano- and microstructures.*

1. Introduction

The formation of laser-induced periodic structures on surfaces of various materials under different conditions of laser irradiation has been investigated for more than 30 years. The formation (in other words, writing) of surface structures under irradiation by laser pulses with a duration of several hundreds of picoseconds or more was studied in detail [1–3]. Such irradiation, with an intensity near the melting threshold, leads to the formation of gratings with a period close to the laser wavelength (for a normally incident laser beam) and multiperiod structures, which are due to the occurrence of various instabilities and capillary waves, on semiconductor and metal surfaces [4, 5]. Irradiation of a material with intensities exceeding its ablation threshold gives rise to quasi-periodic microcones on the surface [6, 7].

In the last decade, a decrease in the surface grating period from the subwavelength scale to several tens of nanometers under ultrashort (femtosecond) laser pulses in the IR range has been demonstrated in many experimental studies [8–13]. One of the reasons for this difference from the effect of sub- and nanosecond laser irradiation is the significant change in the optical properties of surface during its interaction with a single femtosecond laser pulse, because the temperature of the electron subsystem in the surface layer may greatly exceed the lattice temperature [14]; when irradiating semiconductors, a dense electron–hole plasma ($N \approx 10^{21}$–10^{22} cm^{-3}) is intensely generated [15, 16]. Another, no less important difference of the femtosecond laser pulse effect is that the surface relief is written much later after the femtosecond laser pulse is absorbed by the surface [14].

The formation of gratings with periods below the irradiation wavelength on silicon surface in various media by near-IR femtosecond laser pulses was studied in [7, 17–32]. However, the writing of periodic structures on silicon surface by UV femtosecond laser pulses has not been investigated, except for two studies [33, 34], where disordered and ordered microstructures with characteristic sizes much larger than the irradiation wavelength were obtained. All investigations of the silicon surface structuring by UV radiation were performed using nanosecond excimer laser pulses [35, 36].

In this study, along with the frequently used IR femtosecond laser pulses, we also applied femtosecond laser pulses with a wavelength shorter by a factor of about 3, which may be promising for reducing significantly the period of the periodic surface nanostructures at lower nanostructuring thresholds and laser irradiation doses. According to our results, silicon nanostructuring under UV femtosecond laser pulses indeed occurs at lower laser fluences, with the nanostructure period correspondingly reduced (by a factor of about 3).

2. Experimental

The experiments were performed with linearly polarised radiation at the fundamental (central wavelength $\lambda \approx 744$ nm, 12-nm FWHM) and third-harmonic frequencies (central wavelength $\lambda \approx 248$ nm, 1.3-nm FWHM) of a femtosecond Ti : sapphire laser system (Fig. 1). The durations of IR and UV pulses were about 100 fs (in the interaction region); their energies were up to 8 and 0.5 mJ, respectively; the repetition frequency was 10 Hz; and the transverse spatial distribution of the laser field corresponded to the TEM_{00} mode. The laser pulse energy was varied using reflective polarisation attenuators in the corresponding spectral range (Avesta Project) and monitored by a calibrated DET-210 photodiode (Thorlab), exposed to a weak laser spot through a rotational dielectric mirror. The laser energy was chosen so as to avoid significant degradation of laser fluence distribution on the target surface as a result of self-focusing in air and the corresponding effects of chromatic emission, filamentation, and scattering from the air plasma [37].

Micro- and nanostructured areas were written as individual points by focusing the IR (UV) laser radiation into a spot 450 (370) μm in diameter at the intensity level of 1/e under normal incidence on the optically smooth surface of a stationary

A.A. Ionin, S.I. Kudryashov, S.V. Makarov, L.V. Seleznev, D.V. Sinitsyn P.N. Lebedev Physics Institute, Russian Academy of Sciences, Leninsky prosp. 53, 119991 Moscow, Russia;
e-mail: sikudr@sci.lebedev.ru, makarov_sergey_vl@mail.ru;
E.V. Golosov, O.A. Golosova, Yu.R. Kolobov Belgorod State University, ul. Pobedy 85, 308015 Belgorod, Russia;
A.E. Ligachev A.M. Prokhorov General Physics Institute, Russian Academy of Sciences, ul. Vavilova 38, 119991 Moscow, Russia

Received 30 December 2010; revision received 29 June 2011
Kvantovaya Elektronika **41** (9) 829–834 (2011)
Translated by Yu.P. Sin'kov

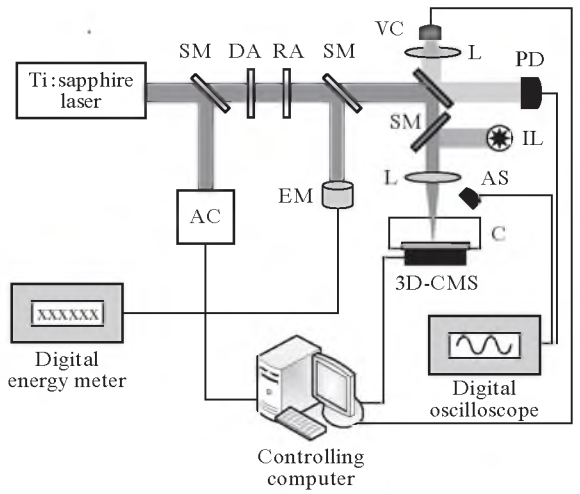

Figure 1. Experimental setup for femtosecond laser nano- and microstructuring of surfaces:
(SM) semitransparent mirror, (DA) diffraction attenuator, (RA) reflection attenuator, (AC) autocorrelator, (PD) photodiode, (EM) thermoelectric energy meter, (L) quartz lens, (VC) video camera, (IL) illumination lamp, (C) glass cell with sample, (3D CMS) 3D controlled motorised micropositioner, and (AS) acoustic sensor.

Si(100) target. The surface images written by a Quanta FEG 600 scanning electron microscope (SEM) were analysed using a fast Fourier transform.

3. Nano- and microstructuring of silicon surface under IR femtosecond laser pulses

Figure 2 shows the three main stages of surface relief transformation: a 1D subwavelength grating (nanograting); isotropic microstructures, which cover partially the 1D subwavelength grating; and an isotropic microstructure. The transition between stages is accompanied by an increase in the number of laser pulses N incident on the sample, at a constant laser fluence F.

For relatively low IR femtosecond laser pulse fluences ($F \approx 0.31$ J cm^{-2}), at the number of pulses $N \approx 100$, one can observe the formation of periodic and quasi-periodic 1D gratings with the average period $\Lambda \approx 550$ nm and the average thickness of protrusions (ridges) $\Delta \approx 290$ nm (Fig. 2a). It can clearly be seen in Fig. 2b that clusters of ablated material arose on the previously formed 1D nanograting. The corresponding spatial Fourier spectra of the surfaces also clearly demonstrate the transition from a quasi-periodic 1D surface nanograting to a 2D microstructure (i.e., the transition from a pattern with narrow high-frequency peaks (Fig. 2d) to a spectrum with a low-frequency ring (Fig. 2f)). The 1D nanograting period somewhat increases on average with an increase in the number of pulses from $\Lambda \approx 550$ nm ($N \approx 100$) to $\Lambda \approx 560$ nm ($N \approx 300$).

Figure 3 shows images of the silicon surface areas nanostructured with the same number of IR femtosecond laser pulses ($N \approx 300$) but at different laser fluences: $F \approx 0.25-0.5$ J cm^{-2}. As in the case where the number of pulses was increased at a constant F, there is a transition from a 1D periodic structure to a 2D disordered one; in addition, there are intermediate stages, which are characterised by the surface Fourier spectrum with not only narrow peaks corresponding to 1D nanogratings but also a low-frequency ring due to the isotropic surface structure of microclusters (Figs 3b, 3c). The insets in Figs 3a–c show how the low-frequency ring transforms from a weak one, with two peaks (which correspond to the transverse grating with a period exceeding the laser wavelength by a factor of about 2.5) into a well-pronounced ring.

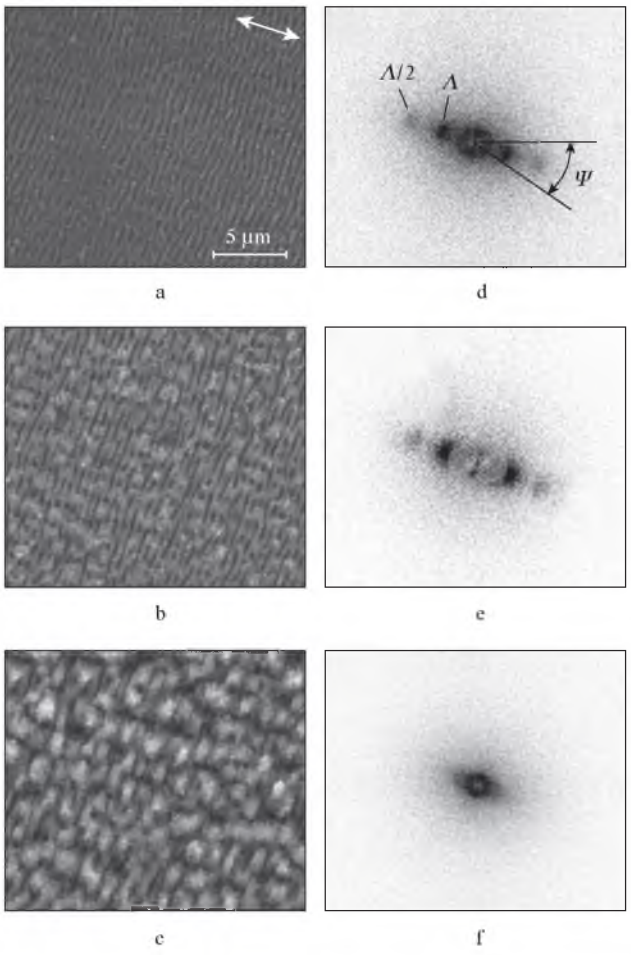

Figure 2. Evolution of a laser-induced subwavelength nanograting of a silicon surface (a) into a microstructure (c) with an increase in the number of pulses N incident on the surface: N = (a) 100, (b) 300, and (c) 1000, at a constant laser fluence: $F \approx 0.31$ J cm^{-2}. The arrow in panel a indicates the orientation of the laser radiation polarisation vector. Panels d–f show the 2D spatial Fourier spectra corresponding to the images in panels a–c, respectively. The symbol Ψ in panel d indicates the angular distribution width for the wave vectors of the surface nanograting with the period $\Lambda \approx 550$ nm.

Thus, both an increase in the number of pulses and an increase in the IR femtosecond laser pulse fluence leads to surface relief roughening. Obviously, in this case we deal with the so-called cumulative effect (where an increase in the number of pulses reduces the threshold laser fluence for implementing a particular structural type and, vice versa, less pulses are necessary for intiating the same processes at a higher laser fluence).

The IR femtosecond laser pulse threshold fluence for forming 1D subwavelength gratings, as a function of the number of pulses N, was determined using the following approximation [38]:

$$F^{\text{nano}}_{\text{IR(UV)}}(N) = F^{\text{nano}}_{\text{IR(UV)}}(1)N^{-\alpha}, \qquad (1)$$

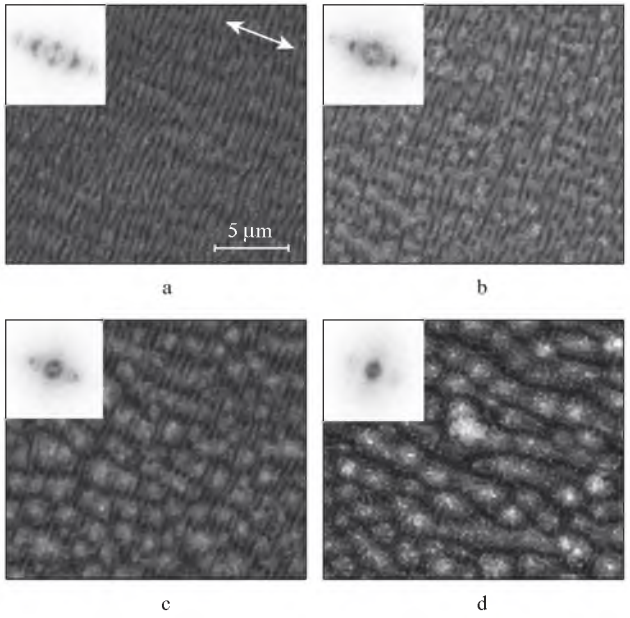

Figure 3. Evolution of the surface structure with an increase in the laser fluence: $F \approx$ (a) 0.25, (b) 0.31, (c) 0.37, and (d) 0.5 J cm^{-2} at $N \approx 300$. The orientation of the laser radiation polarisation is indicated by an arrow. The Fourier spectra of the surface images are shown in the corresponding insets.

where $F_{\mathrm{IR(UV)}}^{\mathrm{nano}}(1)$ is the threshold laser fluence for irradiation by a single IR (UV) femtosecond laser pulse and α is the cumulative parameter, which differs for different materials. Figure 4 shows the experimental values of $F_{\mathrm{IR(UV)}}^{\mathrm{nano}}(N)$, approximated by formula (1); this approximation yields the values $F_{\mathrm{IR}}^{\mathrm{nano}}(1) \approx 0.24$ J cm^{-2} and $\alpha \approx 0.14$, which are close to those measured previously at N in the range from 1 to 100 [39]. The values of the cumulative parameters that are necessary to form isotropic microstructures on silicon surface are $F_{\mathrm{IR}}^{\mathrm{micro}}(1) \approx 0.56$ J cm^{-2} and $\alpha \approx 0.14$.

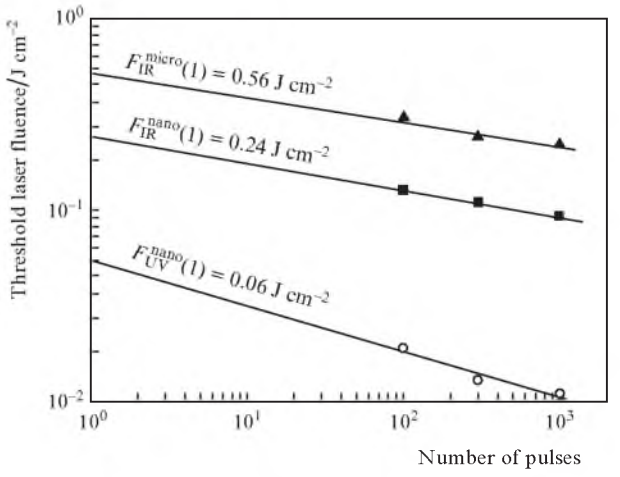

Figure 4. Dependences of the threshold fluence of laser pulses for the formation of surface 1D nanogratings in the IR [$F_{\mathrm{IR}}^{\mathrm{nano}}(N)$] and UV [$F_{\mathrm{UV}}^{\mathrm{nano}}(N)$] spectral ranges and for formation of surface microstructure by IR femtosecond laser pulses [$F_{\mathrm{IR}}^{\mathrm{micro}}(N)$] on the number of laser pulses N: (symbols) measurements in the (▲, ■) IR and (○) UV spectral ranges and (solid lines) approximations by formula (1).

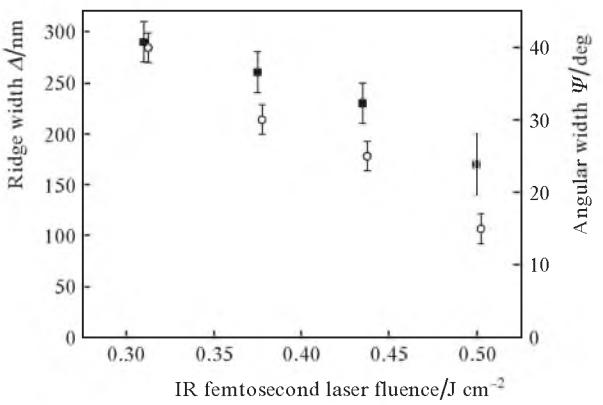

Figure 5. Dependences of the angular distribution width Ψ for the wave vectors of 1D quasi-periodic subwavelength nanograting (○, right axis) and the spatial width Λ of the grating ridge (■, left axis) on the laser fluence of IR femtosecond pulses at $N \approx 100$.

A comparison of the spatial Fourier spectra of different nanostructured areas of the silicon surface showed that the width of the angular distribution of the reciprocal vectors of a 1D nanograting generally decreases with an increase in the number of pulses (Fig. 5); this correlation indicates that a preferred direction is gradually selected for the grating wave vector and promises a higher quality of the 1D nanograting. It was also established that the ridge width in the 1D nanograting decreases with an increase in the IR femtosecond pulse fluence for $N \approx 100$ at a weakly varying period (Fig. 5) and

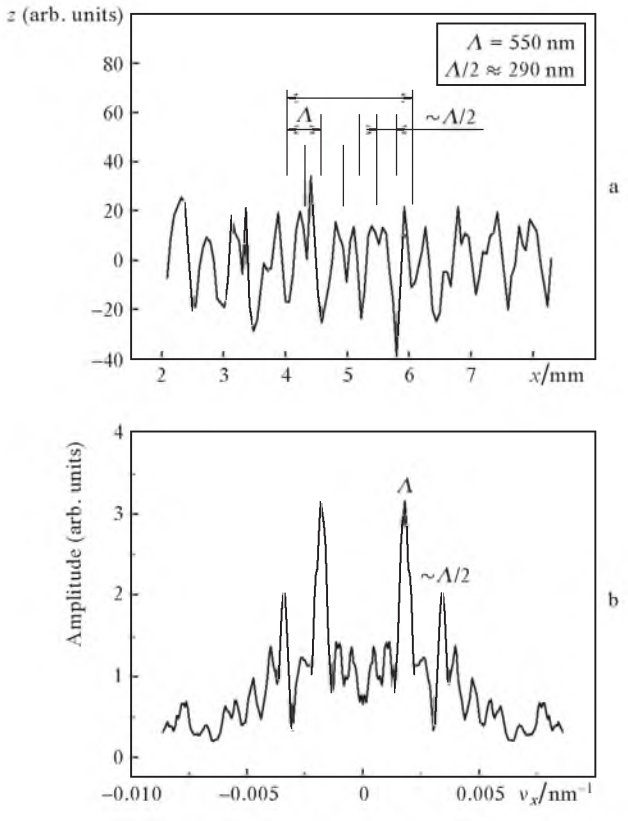

Figure 6. (a) 1D profile of the surface relief and (b) its Fourier spectrum at $F \approx 0.25$ J cm^{-2} and $N \approx 300$. The 2D image of the corresponding relief and its Fourier spectrum are presented in Fig. 3a.

correlates with the increase in the content of ablation products on the surface.

We observed doubling of the surface relief spatial frequency ($\Lambda/2 \approx 290$ nm) in a certain range of IR femtosecond laser pulse external parameters (Figs 2d, 2e, 3a). It is noteworthy that at $F \approx 0.25$ J cm^{-2} and $N \approx 300$ the doubled spatial frequency indeed manifests itself in the profile of periodic surface relief (Fig. 6a) and in its 1D (Fig. 6b) and 2D (Figs 2, 3) Fourier spectra [due to the real writing of a periodic structure with a period smaller than that of the fundamental grating by a factor of 2 (Fig. 6a)]; at the same time, it does not manifest itself in the Fourier spectra because of the anharmonicity of the nanograting profile with a fundamental period of about 550 nm. It is also noteworthy that, at a fixed laser fluence F above $F_{IR}^{nano}(1)$ (for example, at $F \leqslant 0.31$ J cm^{-2}), the second harmonic of the surface relief arose in a certain range of the number of pulses ($100 \leqslant N \leqslant 300$) and then, as was previously observed in [40], disappeared at larger N. Similarly, the second harmonic at $N = 300$ manifested itself in the range $F_{IR}^{nano}(1) \leqslant F = 0.25$–$0.31$ J cm^{-2}. We established for the first time that the relief structure exhibiting the second harmonic disappears under the layer of ablation products redeposited on the surface, as can be seen in Figs 2 and 3.

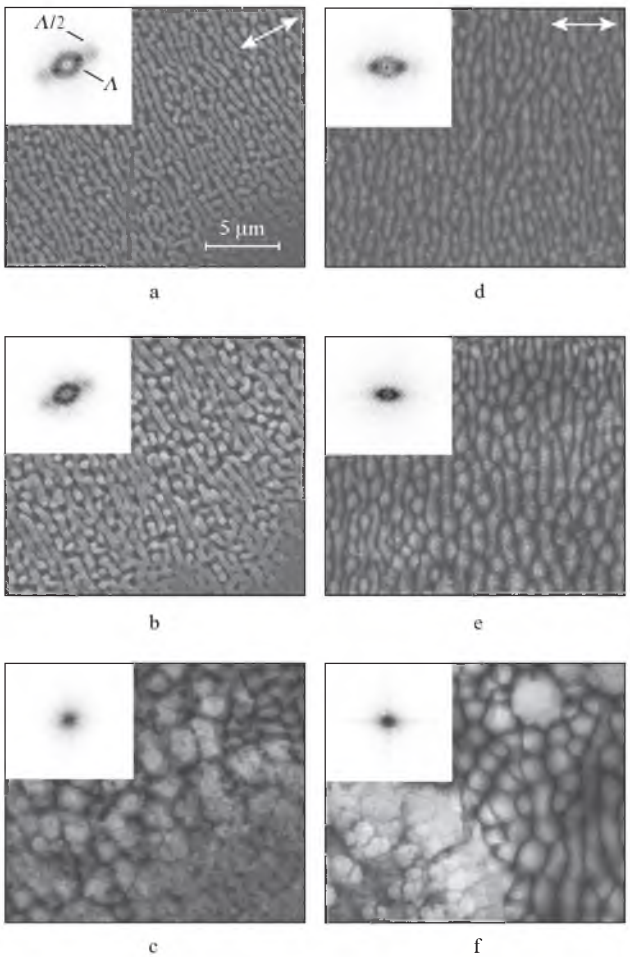

Figure 7. SEM images of silicon surface after irradiation by UV femtosecond laser pulses at $F \approx$ (a–c) 0.09 and (d–f) 0.18 J cm^{-2} for $N \approx$ (a, d) 100, (b, e) 300, and (c, f) 1000 pulses. The orientations of laser polarisation for the left and right panels are indicated by arrows in panels a and d, respectively.

4. Nano- and microstructuring of silicon surface under UV femtosecond laser pulses

A silicon surface irradiated by UV femtosecond laser pulses exhibited nanogratings of three types: a low-frequency grating (with a period much larger than the wavelength, $\Lambda_L > \lambda$), a high-frequency grating (with a period somewhat smaller than the wavelength, $\Lambda_H < \lambda$), and a grating containing the second spatial harmonic with respect to the high-frequency nanograting ($\Lambda_{SH} = 2\Lambda_H$).

The changes in the first-type nanogratings that were caused by changing the number of UV femtosecond laser pulses and the laser fluence are shown in Fig. 7. The relief evolution with an increase in N is similar to that in the above-considered case of nano- and microstructuring by IR femtosecond laser pulses. The 1D-nanograting period somewhat increases with an increase in N: $\Lambda_L \approx 540$ and 600 nm at $N \approx 100$ and 300, respectively (Figs 7a, 7b), and then, at $N \approx 1000$, it degrades into a disordered 2D microstructure (Fig. 7c). However, the 1D structural order is almost retained with an increase in the pulse laser fluence, but the nanograting period changes significantly (Fig. 7d): from $\Lambda_L \approx 540$ nm at $F \approx 0.09$ J cm^{-2} and $N \approx 100$ to a rather wide range of Λ_L values (from 300 nm to 1 μm) at $F \approx 0.18$ J cm^{-2} and $N \approx 100$. The values of the cumulative parameters that provide formation of 1D periodic gratings under UV femtosecond laser pulses are as follows: $F_{UV}^{nano}(1) \approx 0.06$ J cm^{-2} and $\alpha \approx 0.24$ (Fig. 4).

When irradiating silicon surface by UV femtosecond laser pulses with a peak laser fluence $F \approx 0.8$–10 J cm^{-2}, disordered microstructures are formed in the spot centre. Periodic structures of different types are observed at different distances from the centre of the irradiated area. As can be seen in Fig. 8, in the area where the local laser fluence $F \approx 0.2$ J cm^{-2} nanogratings with different periods but identical orientation can be written simultaneously: the low-frequency nanograting period, as in the case considered above, is varied within $\Lambda_L \approx 550$–650 nm, while the high-frequency nanograting has a period $\Lambda_H \approx 200$ nm. With a further increase in the distance from the centre of the irradiated area, one can observe only high-frequency nanogratings with the period $\Lambda_H \approx 200$ nm and lines oriented perpendicularly to the laser beam polarisation (Fig. 9). It can be seen in Figs 9c and 9d that some areas exhibit a pronounced decrease in the period of small-scale nanogratings by a factor of 2, which is related to the genera-

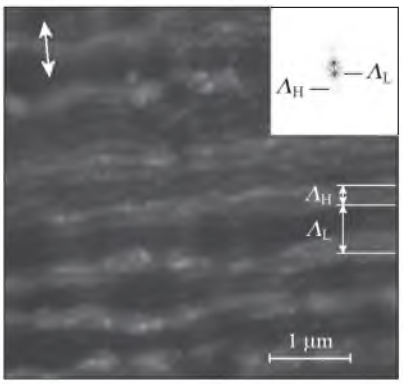

Figure 8. SEM image of a silicon surface area irradiated by UV femtosecond laser pulses at $F \approx 0.2$ J cm^{-2} and $N \sim 10$ and the corresponding Fourier spectrum (inset). The orientation of laser polarisation is indicated by an arrow.

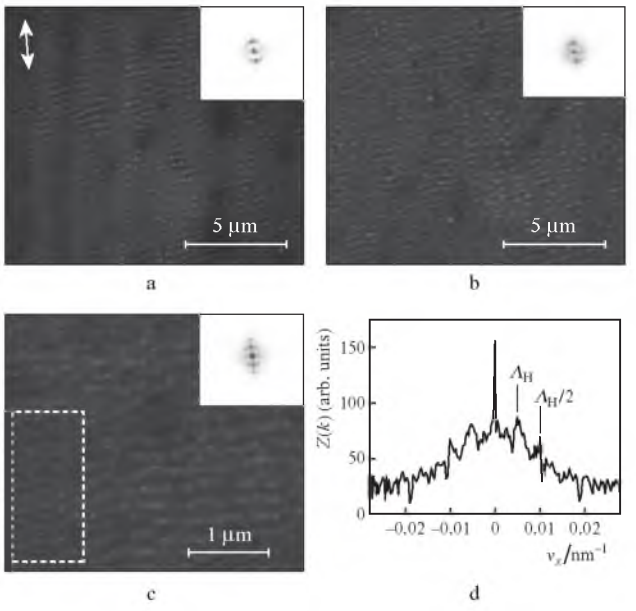

Figure 9. SEM images of silicon surface irradiated by $N \sim 10$ UV femtosecond laser pulses at $F \approx$ (a) 3, (b) 0.8, and (c) 1 J cm^{-2}, with the corresponding 2D Fourier spectra in the insets, and (d) the cross section of the Fourier spectrum in the inset in panel c. The orientation of laser polarisation is indicated by an arrow in panel a; the dotted line in panel c outlines the area where spatial frequency doubling is clearly observed.

tion of the second spatial harmonic of the high-frequency component in the surface relief with $\Lambda_{SH} = 2\Lambda_H$.

5. Discussion

The topological transition of the surface relief with a change in the external radiation parameters (from 1D ordered gratings to isotropic microstructures) is qualitatively the same for IR and UV femtosecond laser pulses, which follows from comparison of Figs 2, 3, and 7. The ridges of the arising 1D surface subwavelength nanogratings are oriented perpendicularly to the laser field polarisation vector for IR and UV femtosecond laser pulses, which is indicative of interference mechanism of formation of these structures [1–3].

The obtained threshold for the formation of periodic 1D nanogratings on silicon surface for a single near-IR femtosecond laser pulse ($F_{IR}^{nano}(1) \approx 0.24$ J cm^{-2}) is somewhat below the melting threshold of the material ($F_{IR}^{melt}(1) \approx 0.3$ J cm^{-2}) [41]. This means that the uniform melting of the surface is of minor importance for the formation of ordered subwavelength relief. The main contribution to the formation of periodic structures on silicon surface in air is from the ablation in the interference maxima of the incident wave and the surface electromagnetic wave excited by it. This is confirmed by the analysis of the SEM images of all structured silicon surfaces subjected to irradiation by IR femtosecond laser pulses (i.e., 1D nanogratings are coated by ablation products in all cases).

At an incident IR laser fluence close to the macroscopic ablation threshold ($F_{IR}^{abl}(1) \approx 0.45$ J cm^{-2} [41]), the F values in the interference maxima in the relief valleys can be rather large due to the local field enhancement. In this case, a large amount of ablated material is redeposited on the surface to form a microcluster structure above the 1D subwavelength gratings (Fig. 2b); this structure corresponds to the low-frequency ring in the Fourier spectrum. The microclusters grow with an increase in both the number of pulses at a constant laser fluence and with increasing laser fluence at a constant number of pulses. This growth is accompanied by an increase in the characteristic distance between the clusters, as is evidenced by the reducing diameter of the low-frequency ring in the corresponding Fourier spectra of the surfaces (Figs 2, 3, 7). Based on the measurements performed, we evaluated the threshold for the microstructure formation: $F_{IR}^{micro}(1) = 0.56N^{-0.14}$ J cm^{-2}; this value exceeds the macroscopic ablation threshold under irradiation by IR femtosecond laser pulses. It should be noted that the exponent α is the same for the formation of both 1D nanogratings and microstructures ($\alpha \approx 0.14$); apparently, this circumstance indicates that the mechanism of diffraction incorporation of the femtosecond laser pulse energy is universal both in the initial stage of formation of nanogratings and during their subsequent degradation.

As was shown in [28], irradiation of silicon surface by several IR femtosecond laser pulses gives rise to narrow ordered valleys; they, in turn, form a surface grating with an anharmonic profile and a period Λ_1, which is determined from relation (2). Under further irradiation of this surface, gratings with the periods $\Lambda_m = \Lambda_1/m \ll \Lambda_1$ [which correspond to the relief spatial frequencies $\nu_x = 1/\Lambda_m = mk_{SW}/2\pi$ [42, 43], where m is a positive integer and k_{SW} is the wave number of the surface electromagnetic wave (SEW)] are formed on it due to the diffraction of the incident laser field. An important factor is that, when comparing the periods of nanogratings written under different conditions, one must compare the periods of their first harmonics [42, 43] rather than the minimum periods or the periods of the strongest harmonics. The main conditions for the formation of surface nanogratings with the periods Λ_m are the condition for SEW excitation on a periodically modulated surface relief and the presence of higher harmonics in its spatial Fourier spectrum (Figs 6b, 9b) [3, 42, 43]:

$$k_{SW} = \frac{2\pi}{\Lambda_1} = \frac{2\pi}{\lambda}\sqrt{\frac{\varepsilon_m \varepsilon_d}{\varepsilon_m + \varepsilon_d}}, \qquad (2)$$

where ε_m and ε_d are, respectively, the complex permittivities of the irradiated material and the adjacent insulator (air); the condition for SEW existence implies that $\mathrm{Re}\,\varepsilon_m < -\varepsilon_d$. The analysis of expression (2) indicates that the subwavelength nanogratings observed by us can be formed under irradiation by both IR ($\Lambda \approx 550$ nm) and UV ($\Lambda \approx 200$ nm) pulses if the real and imaginary parts of the permittivity of photoexcited silicon vary from –1 to –4 and from 0 to 3, respectively. Under irradiation of semiconductors and other nonmetals by femtosecond laser pulses in the visible range, similar permittivity values were observed in many previous experiments as a result of the generation of a dense electron–hole plasma [15, 40, 42–45].

Irradiation by UV femtosecond laser pulses led to the formation of the second spatial harmonic of the surface relief of two types (with the periods $\Lambda_L/2$ and $\Lambda_H/2$). In the former case, the second harmonic was virtually present in the spatial Fourier spectrum (only due to the anharmonic shape of the surface relief cross section). In the latter case, the second spatial harmonic $\Lambda_H/2$ could be observed not only in the 2D surface Fourier spectrum but also in the SEM image (Fig. 9c), as under irradiation by IR femtosecond laser pulses (Fig. 6). In both cases it is only the high spatial frequency (which corresponds to the subwavelength nanograting) that is doubled;

this circumstance indicates the common interference nature of writing these gratings, which was described above.

The formation mechanism of the low-frequency surface nanograting under irradiation by UV femtosecond laser pulses remains unclear, because the previous experiments with other wavelengths did not reveal such structures. A similar situation was observed for only ZnO nanostructuring by 450-fs pulses with $\lambda \approx 248$ nm [46], where the structure period turned out to greatly exceed the wavelength.

One more significant difference between the results of silicon surface structuring using IR and UV femtosecond laser pulses is the absence of ablation traces on the surface exposed to UV laser pulses (Figs 6a, 6b), which can be related to the dominance of photochemical processes occurring on the surface under femtosecond UV laser pulses. Silicon oxides SiO_x are formed in the relief valleys due to the high oxygen content in the atmosphere; these oxides are known to be effectively removed from the surface by UV radiation [36].

6. Conclusions

We compared for the first time the surface structures formed as a result of multipulse IR and UV femtosecond laser pulse irradiation of silicon samples. The SEM analysis of the irradiated surface showed that the evolution of its topology with an increase in the number of pulses is universal for both wavelengths used; i.e., a 1D nanograting is transformed into a 2D isotropic microstructure. This mechanism is confirmed by the spatial Fourier spectra of the corresponding surface images.

The occurrence of the second spatial harmonic of the structured relief is related to the efficient transformation of the incident UV and IR femtosecond laser pulse energy into surface electromagnetic waves on the anharmonic periodic surface relief, which is formed after absorption of few first laser pulses. Further development of the higher spatial harmonics is limited by their mutual competition, which can manifest itself, for example, in redeposition of the ablated material on the surface gratings corresponding to weaker higher spatial harmonics.

Acknowledgements. This study was supported by the Russian Foundation for Basic Research (Project Nos 10-08-00941-a, 11-02-01202-a, and 11-08-01165-a).

References

1. Guosheng Z., Fauchet P.M., Siegman A.E. *Phys. Rev. B*, **26**, 5366 (1982).
2. Sipe J.E., Young J.F., et al. *Phys. Rev. B*, **27**, 1141 (1983).
3. Akhmanov S.A., Emel'yanov V.I., Koroteev N.I. *Usp. Fiz. Nauk*, **147**, 675 (1985).
4. Young J.F., Preston J.S., et al. *Phys. Rev. B*, **27**, 1155 (1983).
5. Young J.F., Sipe J.E., Driel H.M. *Phys. Rev. B*, **30**, 2001 (1984).
6. Dolgaev S.I., Lavrishev S.V., et al. *Appl. Phys. A*, **73**, 177 (2001).
7. Crouch C.H., Carey J.E., et al. *Appl. Phys. Lett.*, **84**, 1850 (2004).
8. Golosov E.V., Emel'yanov V.I., et al. *Pis'ma Zh. Eksp. Tekh. Fiz.*, **90**, 116 (2009).
9. Vorobyev A.Y., Makin V.S., Guo C. *Phys. Rev. Lett.*, **102**, 234301 (2009).
10. Golosov E.V., Ionin A.A., et al. *Ross. Nanotechnol.*, **6**, 59 (2011).
11. Vorobyev A.Y., Guo C. *Appl. Phys. A*, **86**, 321 (2007).
12. Couillard M., Borowiec A. et al. *J. Appl. Phys.*, **101**, 033519 (2007).
13. Borowiec A., Haugen H.K. *Appl. Phys. Lett.*, **82**, 4462 (2003).
14. Agranat M.B., Anisimov S.I., et al. *Zh. Eksp. Teor. Fiz.*, **115**, 675 (1999).
15. Sokolowski-Tinten K., Linde D. *Phys. Rev. B*, **61**, 2643 (2000).
16. Agranat M.B., Anisimov S.I., et al. *Pis'ma Zh. Eksp. Tekh. Fiz.*, **83**, 592 (2006).
17. Crouch C.H., Carey J.E., Shen M., et al. *Appl. Phys. A*, **79**, 1635 (2004).
18. Costache F., Kouteva-Aguirova S., Reif J. *Appl. Phys. A*, **79**, 1429 (2004).
19. Riedel D., Hernandez-Pozos J.L., Palmer R.E., et al. *Appl. Phys. A*, **78**, 381 (2004).
20. Yonekubo H., Katayama K., Sawada T. *Appl. Phys. A*, **81**, 843 (2005).
21. Harzic R.L., Schuck H., et al. *Opt. Express*, **13**, 6652 (2005).
22. Zabotnov S.V., Golovan' L.A., Ostapenko I.A., et al. *Pis'ma Zh. Eksp. Tekh. Fiz.*, **83**, 76 (2006).
23. Hommes V., Miclea M., Hergenroeder R. *Appl. Surf. Sci.*, **252**, 7449 (2006).
24. Tan B., Venkatakrisnan K. *J. Micromech. Microeng.*, **16**, 1080 (2006).
25. Crawford T.H.R., Haugen H.K. *Appl. Surf. Sci.*, **253**, 4970 (2007).
26. Liu Y., Liu S., Wang Y., et al. *Laser Phys.*, **18**, 1148 (2008).
27. Li J.M., Xu J.T. *Laser Phys.*, **19**, 121 (2009).
28. Huang M., Zhao F., Cheng Y., et al. *Opt. Express*, **18**, A600 (2010).
29. Reif J., Varlamova O., Ratzke M., et al. *Appl. Phys. A*, **101**, 361 (2010).
30. Wang C., Huo H., et al. *Nanotechnology*, **10**, 075304 (2010).
31. Bonse J., Kruger J. *J. Appl. Phys.*, **108**, 034903 (2010).
32. Bonse J., Rosenfeld A., Kruger J. *Appl. Surf. Sci.*, **257**, 5420 (2011).
33. Ameer-Beg S., Perrie W., et al. *Appl. Surf. Sci.*, **127**, 875 (1998).
34. Zorba V., Tzanetakis P., et al. *Appl. Phys. Lett.*, **88**, 081103 (2006).
35. Clark S.E., Emmony D.C. *Phys. Rev. B*, **40**, 2031 (1989).
36. Pedraza A.J., Fowlkes J.D., Lowndes D.H. *Appl. Phys. A*, **69**, 731 (1999).
37. Zemlyanov A.A., Ionin A.A., Geints Yu.E., Kudryashov S.I., et al. *Zh. Eksp. Teor. Fiz.*, **138**, 822 (2010).
38. Yong J., Becker M.F., Walser L.M. *J. Opt. Soc. Am. B*, **5**, 648 (1988).
39. Bonse J., Baudach S., et al. *Appl. Phys. A*, **74**, 19 (2002).
40. Bonse J., Munz M., Sturm H. *J. Appl. Phys.*, **97**, 013538 (2005).
41. Kudryashov S.I., Emel'yanov V.I. *Pis'ma Zh. Eksp. Tekh. Fiz.*, **73**, 263 (2001).
42. Golosov E.V., Ionin A.A., et al. *Zh. Eksp. Teor. Fiz.*, **140**, 21 (2011).
43. Golosov E.V., Ionin A.A., et al. *Phys. Rev. B*, **83**, 115426 (2011).
44. Kudryashov S.I., Emel'yanov V.I. *Pis'ma Zh. Eksp. Tekh. Fiz.*, **73**, 751 (2001).
45. Kudryashov S.I., Emel'yanov V.I. *Zh. Eksp. Teor. Fiz.*, **121**, 113 (2002).
46. Museur L., Michel J.P., et al. *J. Opt. Soc. Am. B*, **27**, 531 (2010).